JOURNAL OF GEOPHYSICAL RESEARCH, VOL. 111, D07209, doi:10.1029/2005JD006389, 2006

Optical properties of soot–water drop agglomerates: An experimental study

E. F. Mikhailov,[1] S. S. Vlasenko,[1] I. A. Podgorny,[2] V. Ramanathan,[2] and C. E. Corrigan[2]

Received 18 June 2005; revised 6 October 2005; accepted 13 January 2006; published 15 April 2006.

[1] Black carbon (BC) and organic carbon (OC) are the largest contributors to the aerosol absorption in the atmosphere, yet the absorption cross sections of BC and OC per unit mass are subject to a large uncertainty due to morphology, physicochemical properties, and the mixing state of carbonaceous particles. Theoretical studies suggest the possibility of an enhanced absorption by soot–cloud drop agglomerates; however, the magnitude of the effect has never been measured directly and remains highly uncertain. This study is a laboratory experiment aimed at the modeling of direct radiation forcing due to soot-water interaction in the presence of glutaric acid, a water-soluble OC. Specifically, we generate, in the laboratory, hydrophobic soot (acetylene soot) and hydrophilic soot (mixture of acetylene soot and glutaric acid) and investigate the structural and optical properties of hydrophobic and hydrophilic soot particles in dry and water-saturated air. Hydrophobic soot (HBS) particles do not exhibit any structural or morphological differences under dry and saturated conditions, whereas hydrophilic soot (HLS) particles, i.e., BC with a monolayer of glutaric acid, collapse into globules when relative humidity (RH) is increased to saturation. The optical properties of HBS show very little dependence on RH while HLS scattering and absorption coefficient increase markedly with RH. For the cases considered here, the maximum enhancement in absorption for a soot–water drop mixture was as much as a factor of 3.5, very similar to theoretical predictions. The data provided in this study should advance the treatment of polluted cloud layers in climate models.

Citation: Mikhailov, E. F., S. S. Vlasenko, I. A. Podgorny, V. Ramanathan, and C. E. Corrigan (2006), Optical properties of soot–water drop agglomerates: An experimental study, *J. Geophys. Res.*, *111*, D07209, doi:10.1029/2005JD006389.

1. Introduction

[2] Aerosol pollution (or haze) is a widespread phenomenon typical to many industrial regions, as well as rural areas in the tropics and subtropics subjected to heavy biomass burning [e.g., *Ramanathan et al.*, 2001a; *Anderson et al.*, 2003]. The direct radiative impact on the Earth's radiative balance, referred to as direct forcing, is estimated from chemical transport models [e.g., *Kinne et al.*, 2003, and references therein] or directly from observations during aerosol field campaigns [e.g., *Jayaraman et al.*, 1998; *Russell et al.*, 1999; *Satheesh and Ramanathan*, 2000; *Ramanathan et al.*, 2001b; *Huebert et al.*, 2003]. The impact of aerosols on cloud properties [*Twomey*, 1977] and cloud amount [*Ackerman et al.*, 2000] invariably require models of clouds and radiation. Aerosol impact on the Earth's climate is estimated from global climate models [e.g., *Hansen et al.*, 1997; *Jacobson*, 2001; *Wang*, 2004, and references therein]. It has become evident over the last decade that absorbing aerosols play a crucial role in impacting global [*Intergovernmental Panel on Climate Change*, 2001] and regional climate, especially hydrological cycles [*Ramanathan et al.*, 2001a]. Mineral dust and carbonaceous aerosols (mostly black carbon (BC), also known as elemental carbon, and also organic carbon (OC)) are the largest contributors to aerosol absorption in the atmosphere. Observed values for the BC specific attenuation cross section range from 4 to 20 m^2/g [*Liousse et al.*, 1993]. While a significant part of this spread is due to the use of different methods and definitions with respect to BC absorption cross sections, it also reflects a great deal of variability due to morphology, chemical and physical properties and mixing state of carbonaceous aerosol.

[3] Carbonaceous particles are a by-product of liquid or gaseous fuel combustion and are also known as soot [*Seinfeld and Pandis*, 1998]. In general, soot consists of small spherical primary particles (also known as spherules or monomers) combined into branched aggregates. The monomers have the mean size of tens of nanometers and are composed of amorphous BC mixed with some amount of OC and other elements. The mass ratio of these components fluctuates for different fuel types and burning conditions [e.g., *McDow et al.*, 1996; *Finlayson-Pitts and Pitts*, 2000; *Lim et al.*, 2003; *Schauer et al.*, 2003]. As the soot particles age in the atmosphere, they are mixed with other

---

[1] Atmospheric Physics Department, Research Institute of Physics, St. Petersburg State University, St. Petersburg, Russia.

[2] Center for Atmospheric Sciences, Scripps Institution of Oceanography, University of California, San Diego, La Jolla, California, USA.

0148-0227/06/2005JD006389$09.00

particles (e.g., sulfates) through coagulation, condensation of secondary aerosol compounds and cloud processing. Over a timescale of a few days, the aging process eventually leads to an internal aerosol mixture. [*Seinfeld and Pandis*, 1998]. The transformation of soot and soot-containing aerosols has been studied using single particle analysis, transmission electron microscope (TEM) imagery and other techniques during aerosol campaigns [e.g., *Ramanathan et al.*, 2001b; *Maria et al.*, 2002; *Guazzotti et al.*, 2003; *Maria et al.*, 2003] and in the laboratory [e.g., *Weingartner et al.*, 1997; *Corrigan and Novakov*, 1999; *Mikhailov et al.*, 2001; *Schnaiter et al.*, 2003]. While pure BC particles tend to be hydrophobic, coating of BC particles with organic compounds may change their hygroscopic properties [*Russell et al.*, 2002] and hence lifetime in the atmosphere. Our lack of understanding of these processes makes a quantitative estimate of the atmospheric lifetime of carbonaceous particles difficult [*Seinfeld and Pandis*, 1998].

[4] Radiative transfer modules used in most climate models are based on Mie theory, i.e., assuming spherical shape for the particles. While this approach is appropriate for cloud drops in unpolluted regions and aqueous sulfate particles, it is questionable for soot and soot-containing aerosol and cloud drops; therefore far more advanced computational techniques are needed [*Fuller et al.*, 1999; *Sorensen*, 2001, and references therein]. According to *Fuller et al.* [1999], for example, aggregation alone may increases BC absorption by 30% whereas encapsulation of soot particle within a sulfate host may further increase BC absorption by the factor of 2. Furthermore, soot randomly positioned within sulfate particles may increase BC absorption by the factor of about 2.5–4.0. While the majority of global climate models [e.g., *Wang*, 2004, and references therein] treat BC as externally mixed, the use of the internal mixing approximation for BC-sulfate mixtures [e.g., *Haywood et al.*, 1997] or approximating aerosol as a BC core concentrically located within sulfate particle [e.g., *Jacobson*, 2000] result in a stronger radiative heating by BC on global scales. Further studies are therefore needed to close the gap between theoretical calculations of BC absorption cross sections, observations of BC mixing state during aerosol field campaigns, and climate modeling.

[5] Cloud processing results in a restructuring of fresh soot particles and a change in BC absorption cross sections [*Liousse et al.*, 1993]. The all-sky aerosol radiative forcing is further impacted by interaction between soot and soot-containing aerosol with water drops. With fractal soot clusters residing inside the water drops, the soot–water drop agglomerates may work as optical resonators increasing BC absorption cross sections (e.g., theoretical calculations by *Markel and Shalaev* [1999] and *Markel* [2002]). The preferential BC particle location on the top or close to the bottom of the droplet can also result in an increased absorption [*Chylek and Hallett*, 1992; *Chylek et al.*, 1996]. Both effects critically depend on hygroscopicity of aerosol particles and hence the type of the fuel burned and combustion properties. For example, wetted carbon aggregates collapse to a compact structure during hygroscopic growth, whereas diesel combustion particles exhibit a much weaker restructuring [*Weingartner et al.*, 1997]. While the theoretical studies hint at an enhanced absorption due to encapsulation of soot particle within a cloud drop, the magnitude of the effect remains highly uncertain and necessitates further research.

[6] The goal of this paper is to present direct measurements of optical properties of the soot–water drop system using laboratory equipment specifically designed to measure the optical coefficients of internally mixed particles in the humid conditions [*Mikhailov et al.*, 2003]. In addition, we present the results of TEM measurements of soot particles to establish a relationship between optical parameters of soot–water drop agglomerates and structural parameters of soot particles.

2. Experimental Setup

[7] The laboratory facilities employed in this study provide generation, modification and optical measurements of soot particles under humid conditions (Figure 1).

[8] Soot particles are generated with a diffusion acetylene burner, preventing preliminary mixing of the fuel and oxidizer [*Samson et al.*, 1987; *Mulholland and Choi*, 1998] and resulting in an incomplete combustion of acetylene (>99.1%, volume flow 1 cm^3/s). This operation mode provides a stable and reproducible mechanism of soot generation. The diffusion flame is a laminar stream (approximately 30 cm long) producing a high concentration of primary particles. Coagulation of the primary particles leads to formation of micron size soot fractal aggregates. An orifice mounted at the top of the burner turbulizes airflow and provides uniformly mixed soot in the volume by reducing soot concentration and preventing further coagulation of the particles. Mass concentration, size and structure of soot aggregates are a function of volume rates of air and acetylene.

[9] The hydrophilic properties of the fresh soot particles are further modified by condensing glutaric acid vapor at the surface of the particles in a ring gap-mixing nozzle. Glutaric acid, as well as other low-molecular-weight dicarboxylic acids, are water soluble OC emitted either directly into atmosphere as a result of biomass and fuel burning or indirectly as a reaction product of the primary volatile OC [*Lawrence and Koutrakis*, 1996; *Finlayson-Pitts and Pitts*, 2000; *Fuzzi et al.*, 2001; *Peng et al.*, 2001; *Yao et al.*, 2002]. Because of hygroscopicity [*Saxena and Hildemann*, 1996; *Prenni et al.*, 2001, 2003], an adsorption of glutaric acid vapor by the soot surface transforms the particle from hydrophobic to hydrophilic. For this purpose, airflow is enriched with glutaric acid vapor by blowing the gas over the surface of solid/liquid glutaric acid at 94°–110°C inside a thermostatically controlled evaporator and then mixed with sample air containing fresh soot aerosol [*Niessner and Helsper*, 1985]. After condensation onto the soot particles, the excess glutaric acid vapor is adsorbed in the 100 cm length annular diffusion denuder filled with activated charcoal. The resultant hydrophilicity of soot particles is a function of glutaric acid temperature and aerosol mass flow inside the evaporator. In this paper, the results of optical measurements are reported for fresh hydrophobic soot (hereafter referred to as HBS), surface-modified hydrophilic soot (HLS) and highly hydrophilic soot (HHLS) particles. HLS have a constant glutaric acid to soot mass ratio about of 0.02, while HHLS have a variable ratio from 0.02 to 2.

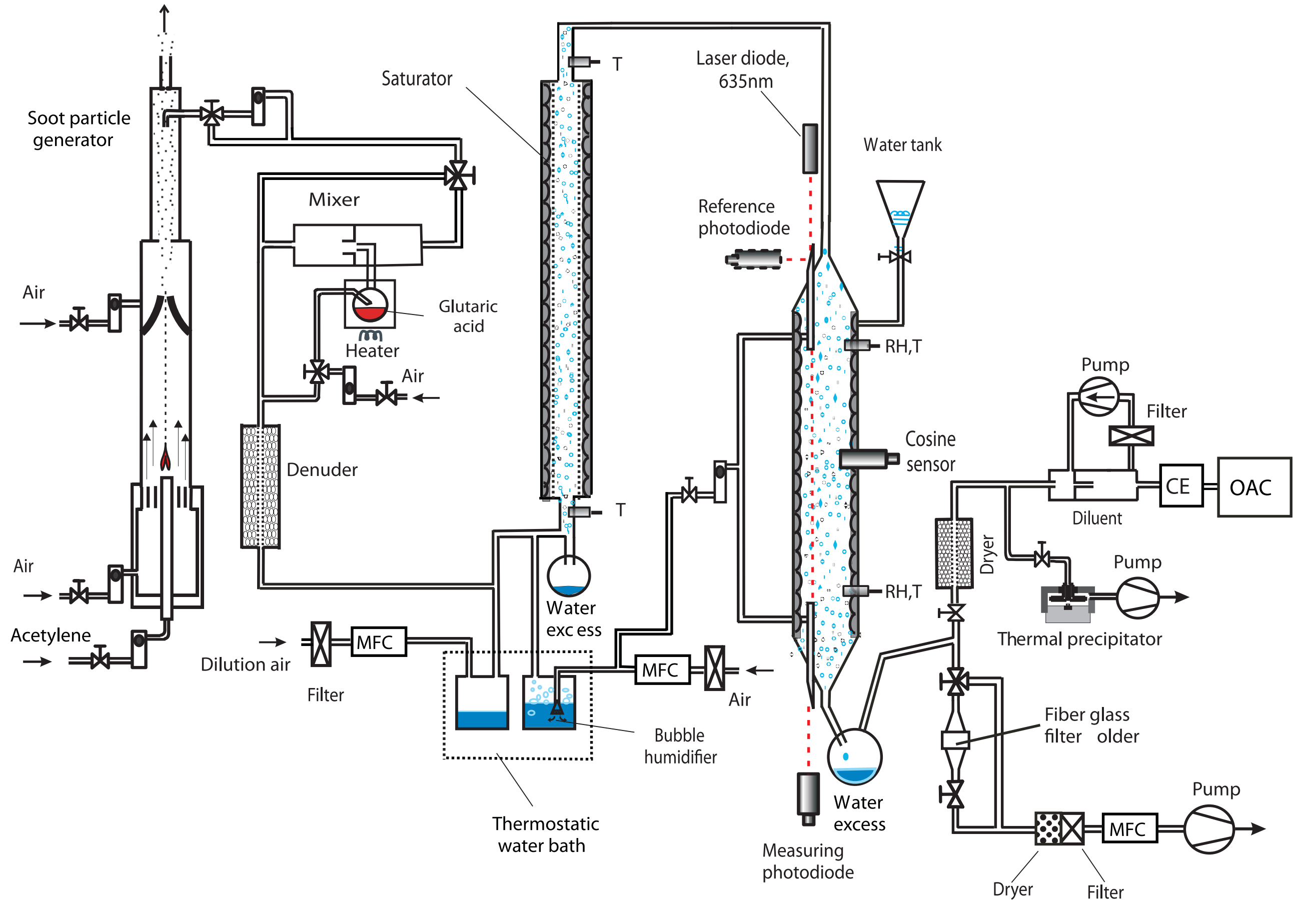

Figure 1. Experimental setup: RH and T are relative humidity and temperature of the sensors, respectively, MFC is mass flow controller, CE is condensation enlarger, and OAC is optical aerosol counter.

[10] Wetted soot particles are generated in a thermostatic saturator 1.5 cm in diameter inside and 110 cm long. The inner walls of the saturator are covered with a hygroscopic fabric. To hold constant saturation conditions, a clean airflow is first bubbled through water and then fed to the saturator. The temperature of water in the bubbler is kept at 42°C. The soot-water mixture is then supplied to the optical cell via a 5-cm-long heat-insulated connection tube. The optical cell is made of duralumin, 7.5 cm in diameter inside and 124 cm long including entrance and exit cones. The inner walls of the optical cell are covered with light-absorbing hygroscopic fabric continually moistened by water flowing from a container mounted at the top of the cell. Excess water is collected in a tank at the bottom of the cell, while the compressor pumps out the excess aerosol. Both saturator and optical cell are equipped with a thermostat system. To provide constant moisture content, the thermostatic conditions of the cell are adjusted so that the temperature of output flow from the saturator is equal to the flow temperature inside the cell. Thermocouples (Voltcraft 502, accuracy ±0.2 K, precision ±0.1 K) are used to measure the temperature of input and output flows in the saturator.

[11] Capacitive humidity sensors (RH and T shown in Figure 1, MHT-7 made in Russia) were used to measure relative humidity (RH = 10–99%, accuracy ±2% RH) and temperature (accuracy ±0.5 K) of the aerosol flow inside the optical cell. Under saturated conditions, relative humidity was determined by weighing the mass of water absorbed by silica gel cartridge (3.0 cm in diameter, 14 cm long).

[12] To ensure that all of the water vapor contained within the airflow (6.0 L/min) was absorbed, the output of the silica gel cartridge was monitored with an additional humidity sensor. On the basis of ideal gas law, the measured mass of water was recalculated into RH. The relative error in retrieving the saturated water vapor pressure was 1.7%.

[13] The soot mass concentration is measured by weighing (micro balance, Kern 770) of the deposited particles on 4.7 cm fiberglass filters (Macherey-Nagel) with an accuracy of 0.01mg. For the measurement reported in this paper, the sampling time was less than 10 min and the deposited mass of aerosol was within 0.04–5.0 mg. Before weighing, both pure and exhibited filters were kept dry for 10 hours. The gravimetric method was also used to measure the mass concentration of adsorbed/condensed glutaric acid, which had sampling times of about 40 min. The mass of glutaric acid was determined as a difference between the mass of exposed filters before and after heating at 430 K in a vacuum tank (residual pressure $\sim 10^{-3}$ torr) for 4 hours. A thermogravimetric analysis of original acetylene soot showed only a 4% loss in weight when soot was heated to 430 K.

[14] Aerodynamic stability of all streams and reproducibility of the aerosol dispersion system are achieved with the use of mass flow controllers, D-5111 and D-6211 (Mess und Regeltechnik GmbH). The optimum stream modes were selected as following: 6 L/min in the bubbler, 12 L/min in the optical cell and 0.1–1.0 L/min for the air sampling from the acetylene burner.

[15] The collimated laser beam at 635 nm (3-mW laser diode) is used as a light source for the optical cell. The intensity of transmitted light is measured with a silicon photo diode placed into a light-protective cylinder. Entrance and exit glass windows of cell are positioned under the Brewster's angles. To prevent particle deposition, clean air with a flow rate of 0.4 L/min purges the optical windows. Intensity of the light reflected from the entrance window (and hence the incident light intensity) is measured with a reference photodiode.

[16] In addition to light extinction measurements, total scattering is measured with an integral cosine sensor. The sensor, a silicon photo diode with active surface 0.95 cm^2, is positioned at the center of the cell 10 mm away from the laser beam and collects light scattered from 1.2° to 178.8° [*Mulholland and Bryner*, 1994]. The electrical signals from photo diodes carry on to buffer amplifiers and then to a personal computer to be processed. Instant values of optical depth, extinction and scattering coefficients, and aerosol concentration are continuously displayed on the monitor.

[17] Particle number concentration is measured with an optical aerosol counter (OAC-3, Russian). Before entering the counter, aerosol is diluted with clean dry air in proportion of 1:1 $\div$ 5 ($\times 10^3$) and goes to the condensation enlarger (CE) where dry particles grow as a result of condensation of supersaturated dibutyl phthalate vapor to form optically detectable droplets [*Sutugin and Fuchs*, 1965; *Baron and Willeke*, 2001].

[18] The structural parameters of soot are derived from TEM observations. For this purpose, a fraction of the downstream flow is pumped through the thermal precipitator. The particles are then sampled on the 3 mm nickel grids covered with a formvar film. To calibrate TEM magnification the polystyrene latex 83 ± 2.7 nm and 0.503 ± 0.015 μm (Postnova analytics) were used. In addition, a sorptograph technique (Model ADS-1B, Shimadzu) is employed to determine specific surface area and the water adsorption isotherm of soot particles. The specific surface area is obtained on the basis of BET theory with nitrogen as the adsorbate. Water adsorption isotherms were measured at 298 K by an elution method [*Greg and Sing*, 1984]. The measured specific surface area of initial nonmodified soot particles was 31.5 ± 0.5 m^2/g.

3. Optical Properties of Aerosols

[19] Optical depth and volume extinction coefficient are derived from the Beer-Lambert law:

$$I = I_0 \exp(-\tau) = I_0 \cdot \exp(-K_{ext} \cdot L) = I_0 \cdot \exp(-k_{ext} \cdot cL), \quad (1)$$

where I is the light intensity, τ is the optical depth, K_{ext} is the volumetric extinction coefficient, L = 1 m is the length of the optical cell, k_{ext} is the specific mass extinction coefficient, and c is the mass concentration of aerosol particles ($\mathrm{g/m}^3$) in the cell. I_0 is the intensity of light passed through the cell without aerosol. The I values were found to vary linearly with the electric signal at the buffer amplifier, so that optical depth was calculated as

$$\tau = -\ln\frac{I}{I_0} = -\ln\frac{V^{phd}}{V_0^{phd}}, K_{ext} = \frac{\tau}{L}, k_{ext} = \frac{\tau}{cL}, \quad (2)$$

where V^{phd} and V_0^{phd} are the measured voltages with and without aerosol, respectively. The total scattering coefficient was measured with cosine sensor [*Patterson et al.*, 1991; *Mulholland and Bryner*, 1994]. An ideal response of the sensor is proportional to the cosine angle of the incident laser beam; however, the real sensor deviates slightly from the cosine law with the magnitude of the deviation being less than 1%. The difference between the signals from the cells with and without aerosol, $\Delta V^{cs} = V_{aerosol}^{\cos.sensor} - V_{clear}^{\cos.sensor}$, is proportional to

$$\Delta \mathrm{V}^{\mathrm{cs}} = \xi_{\mathrm{cal}} \cdot \mathrm{V}_0^{\mathrm{phd}} \cdot \mathrm{K}_{\mathrm{sca}} \quad (3)$$

The proportionality coefficient ξ_{cal} was determined by the calibration carried out on nonabsorbing particles (polystyrene latex or water droplets) for which $K_{ext} = K_{scat}$. Applying equation (3) to nonabsorbing particles yields

$$\xi_{cal} = \frac{\Delta V^{cs}}{V_0^{phd} \cdot K_{ext}}. \quad (4)$$

Thus, for absorbing aerosols, the change in the intensity of the transmitted light allows determination of the extinction coefficient from equation (2), while the measurements at the cosine sensor allow obtaining the scattering coefficient as

$$\mathrm{K}_{\mathrm{sca}} = \xi_{\mathrm{cal}}^{-1} \frac{\Delta \mathrm{V}^{\mathrm{cs}}}{\mathrm{V}_0^{\mathrm{phd}}}. \quad (5)$$

The volumetric absorption coefficient and single scattering albedo (SSA) are calculated as

$$\mathrm{K}_{\mathrm{abs}} = \mathrm{K}_{\mathrm{ext}} - \mathrm{K}_{\mathrm{scat}} \quad (6)$$

and

$$\omega = \frac{K_{sca}}{K_{ext}}. \quad (7)$$

In addition, under known accounting particles concentration N, the integral cross sections C_{ext}, C_{abs} and C_{sca} can be calculated as

$$C_i = \frac{K_i}{N}, \quad (8)$$

where index i denotes extinction, absorption or scattering. Accordingly, for specific scattering and absorption coefficients,

$$k_{sca} = \frac{K_{sca}}{c}, k_{abs} = \frac{K_{abs}}{c}, \quad (9)$$

It should be noted that the scattered light collected by the cosine sensor falls into the 1.2° to 178.8° range instead of ideal of 0°–180°, thus underestimating the magnitude of scattered radiation. The relative errors due to this effect were estimated both for soot particles on the basis of RDG approximation for fractal aggregates [*Koylu and Faeth*, 1994] and for water droplets using Mie codes [*Bohren and Huffman*, 1998]. For the size range of interest, the relative errors for both soot and water droplets do not exceed 2%.

4. Microstructure and Mass Concentration of Aerosols

4.1. Microstructure and the Mass Contents of Soot Particles

[20] As mentioned earlier, soot consists of small spherical primary particles (spherules) combined into branched aggregates. The primary particles, or monomers, have a mean size of tens of nanometers and are composed of amorphous elemental carbon mixed with some amount of high molecular hydrocarbons. The mass ratio of these components is a function of fuel type and burning conditions [*McDow et al.*, 1996]. The acetylene soot contains about 94% pure carbon and is hydrophobic as a result.

[21] Fractal analysis is a common approach used to quantify the structure of soot aggregates [e.g., *Mikhailov et al.*, 2001, and references therein]. The most useful quantity for fractal analysis is mass fractal dimension D_f, defined as a scaling relation between number of primary particles in aggregate N and gyration radius R_g:

$$N = k_f \left(\frac{R_g}{r_p}\right)^{D_f}, \tag{10}$$

where r_p is the radius of primary particles, k_f is the so-called fractal prefactor related to the packing density of particles in the aggregate. The gyration radius can be computed as

$$R_g^2 = \frac{\sum_{i=1}^{N} \nu_i \mathbf{r}_i^2}{\sum_{i=1}^{N} \nu_i}, \tag{11}$$

where r_i is the radius vector of ith spherule with respect to the cluster center of mass, and ν_i is the volume of the same spherule.

[22] Another method to calculate fractal dimension is based on the direct application of the Hausdorf-Bezikovich (HB) dimension [*Mandelbrot*, 1983] to the digital image of the fractal cluster. At each algorithm step, the digital image is divided into an array of equal squares with the side ε. The number of squares with at least one nonempty pixel N_b is a function of ε

$$\mathrm{N_b}(\varepsilon) \propto \varepsilon^{-\mathrm{D_b}}. \tag{12}$$

The fractal dimension D_b calculated from equation (12) is sometimes called a box (or cell) fractal dimension.

[23] According to the theory of fractal objects, dimension D_f calculated from equation (10) should be the same as HB dimension; however, a set of aggregates of various sizes and with the same fractal dimension is required to determine D_f. This last assumption may be a rough approximation, as different stages of coagulation growth correspond to different dimensions. It means that the use of equation (10) provides a net fractal dimension for an ensemble of polydisperse clusters. At the same time, the size of the box (equation (12)) can be determined for each aggregate separately providing fractal dimension distribution for the ensemble of aggregates.

[24] As mentioned above, the structural parameters of soot aggregates were derived from TEM observations using digital camera and special software for image processing. For given aerosol samples, typical image resolution was ~10 nm per pixel.

[25] As the TEM method deals with the 2-D images of 3-D clusters, correction coefficients for R_g and N in equation (10) are used to account for projectional distortions [*Samson et al.*, 1987; *Cai et al.*, 1993]. The evaluation of 3-D structural parameters of soot particles from 2-D TEM images followed the algorithms of planar fractal analysis described by *Koylu et al.* [1995].

[26] The TEM projections were also used for determination of size distribution as a function of Ferret diameter d_F. d_F is the geometric average of maximum and minimum projection length of a particle. The evaluation of the particle size distribution and the calculation of mean values of the structural parameters were carried out on the basis of about 1000 digital images of the soot aggregates.

[27] The mass concentration of soot was determined directly from filter weighting:

$$c_{soot} = \frac{m_{soot}}{Q\Delta t}, \tag{13}$$

where m_{soot} is the mass of soot deposited on the filter, Q is the flow rate of air passed trough the filter (12 L/min), and Δt is the sampling time.

4.2. A Mixed Particle as a Stratified Sphere

[28] The dry internally mixed particles can be presented as a BC core surrounded with a nonabsorbing glutaric acid shell. Quantitatively, this assumption can be described by

$$\frac{H_{G.A.shell}}{R_{soot\ core}} = \left(\frac{m_{dry}}{m_{soot}} \frac{0.637\rho_{soot}}{\rho_{dry}}\right)^{1/3} - 1, \tag{14}$$

where $H_{G.A.shell} = R_{dry} - R_{soot\ core}$ is the volume equivalent thickness of the glutaric acid shell around the core with equivalent radius, $R_{soot\ core}$, and a factor of 0.637 [*Feder*, 1988] taking into account a random distribution of primary soot spherules in the globules formed as a result of restructuring. $m_{dry}/m_{soo\mathrm{t}}$ is the mass ratio dry mixed particle to mass of soot core, and ρ_{dry} is the specific density of the mixed particle which is given by

$$\rho_{dry} = \left(\frac{x_{G.A.}}{\rho_{G.A.}} + \frac{x_{soot}}{0.637\rho_{soot}}\right)^{-1}, \tag{15}$$

where $x_{GA,}$, x_{soot} and ρ_{GA}, ρ_{soot} are the mass fractions and densities of components in the mixed particle, respectively. In equations (14) and (15) all mass-dependent parameters can be obtained from thermogravimetric measurements. For acetylene soot and glutaric acid, specific densities are ρ_{soot} = 1.9 g/cm^3 [*Dobbings et al.*, 1994] and ρ_{GA} = 1.42 g/cm^3 [*Tao and McMurry*, 1989], respectively.

4.3. Hygroscopic Growth of an Internally Mixed Particle

[29] The water content of the glutaric acid coating depends on RH. At equilibrium the particle diameter of the mixed particle can be described by a growth factor $g(RH)$ as follows [*Pitchford and McMurry*, 1994]:

$$g(RH) \equiv \frac{D_{RH}}{D_{dry}} = \left[1 + \upsilon\left(g_{sol}^3(RH) - 1\right)\right]^{1/3}, \qquad (16)$$

where D_{RH} and D_{dry} are the humid and dry volume equivalent diameters, respectively, υ is the soluble water fraction, and $g_{sol} = D_{sol}/D_{dry,sol}$ is the growth factor of a pure soluble particle. The volume fraction of glutaric acid, υ_{GA} in dry particle can be expressed through the masses and densities of components as follows:

$$\upsilon_{G.A.} = \left[\left(\frac{m_{soot}\rho_{G.A.}}{m_{G.A.}0.637\rho_{soot}}\right) + 1\right]^{-1}. \qquad (17)$$

In the hydration shell term $H_{water\ shell} = R_{RH} - R_{soot\ core}$ from equations (16) and (17) we obtain

$$\frac{H_{water\ shell}}{R_{soot\ core}} = \left(1 + g_{sol}^3 \cdot \frac{0.637\rho_{soot}}{\rho_{G.A.}} \cdot \frac{m_{G.A.}}{m_{soot}}\right)^{1/3} - 1. \qquad (18)$$

The growth factor g_{sol} of pure glutaric acid particles at RH = 10% is 1; in saturated area (RH = 99.5%) it equals 3.802 [*Peng et al.*, 2001]. Detailed data about hygroscopic properties of glutaric acid are available at http://ihome.ust.hk/~keckchan/hygroscopic.html.

5. Experimental Results

[30] We used two humidity modes in the cell to investigate microstructure and optical parameters of the soot particles:

[31] 1. In the "dry" cell mode, airflow was allowed to pass through the dryers, the walls of cell were not humidified, and the bubbling in diluting stream was not used. The relative humidity in the cell was around 10%.

[32] 2. In the "saturated" cell mode, the diluting stream of air was bubbled through a layer of warm water, the entrance flow was saturated, and the walls of the cell were constantly humidified. The relative humidity in the cell was ~100%.

5.1. Microstructure and Size Spectra of Soot Particles

[33] Figure 2 shows the characteristic structure of soot aggregates sampled downstream of the optical cell at both dry and saturated conditions. Figures 3 and 4 display the results of digital processing of particle images. The fractal dimension spectra (Figure 3) illustrate the box dimension (D_b). In this case, the fractal dimension was computed separately for each soot aggregate using equation (12). The soot size distributions are presented in Figure 4 as a function of Ferret diameter. The average values of structural parameters are summarized in Table 1.

5.1.1. Hydrophobic Soot (HBS)

[34] As seen from Figure 2a, 2c, and 2e, the nonmodified acetylene soot is an assembly of a large number of superfine primary particles. During the experiments reported in this study, the average size of primary particles was 41 ± 8 nm. The lack of structural differences under dry (Figure 2a) and saturated (Figure 2b) conditions suggests the hydrophobic nature of primary particles. No substantial difference was found between fractal (Figure 3a) and size spectra (Figure 4a) of the sampled particles.

5.1.2. Hydrophilic Soot (HLS)

[35] As mentioned earlier, the hydrophilic particles were generated by condensing glutaric acid vapor onto fresh acetylene soot. For HLS, the glutaric acid to soot mass ratio was maintained at a constant value of 0.020 ± 0.005. This corresponds to approximately one monolayer of glutaric acid. The mass of the monolayer was estimated as

$$\sigma_{GA} = \frac{S_{soot}}{S_{GA}}\rho_{GA}V_{GA} = \frac{2}{3}S_{soot}\rho_{GA}d_{GA}, \qquad (19)$$

where S_{soot} is the specific surface area of primary soot particle, V_{GA}, S_{GA} and d_{GA} are volume, surface area, and diameter of a glutaric acid molecule, respectively. Inserting S_{soot} = 31.5 m^2/g, d_{GA} = 0.626 nm and ρ_{GA} = 1.42 g/cm^3 to equation (19) yields σ_{GA} = 0.019 (gram glutaric acid/gram soot).

[36] Figures 2a and 2c show that under dry conditions, the surface-modified soot is identical to the original hydrophobic structure. Their fractal (Figures 3a and 3b) and size spectra (Figures 4a and 4b) also resemble each other. At the same time, substantial differences between properties of hydrophilic and hydrophobic soot are clearly noticeable under the saturated conditions. Figure 2d presents the structure of the hydrophilic soot at RH = 100%. It is evident that after wetting, the structure of hydrophilic soot changes dramatically when compared to that of soot at dry conditions. The hydrophilic soot particles have collapsed into globules.

[37] The straightforward explanation of the observed structural transformation is that the soot surface contains active nuclei sites that stimulate the growth of water droplets. As a consequence, the soot particles penetrate easily inside the droplet. During the droplet growth and subsequent evaporation, the water surface tension forces reshape the particle by collapsing the branched structures and ultimately forming a more dense globular shape.

[38] The restructuring of HLS aggregates can be characterized through the change of fractal dimension distribution and size spectrum. Figure 3b shows that the fractal dimension distribution of wetted hydrophilic soot particles tends to shift to larger dimensions compared to that under dry condition. At the same time, the size spectrum of humidified HLS particles tends to move toward smaller sizes because of the densification (Figure 4b).

5.1.3. Highly Hydrophilic Soot (HHLS)

[39] Figures 2e, 2f, 3c, and 4c show the characteristics of hydrophilic soot. The particles had a glutaric acid to soot mass ratio of 1. As seen from Figure 2e, the mixed particles

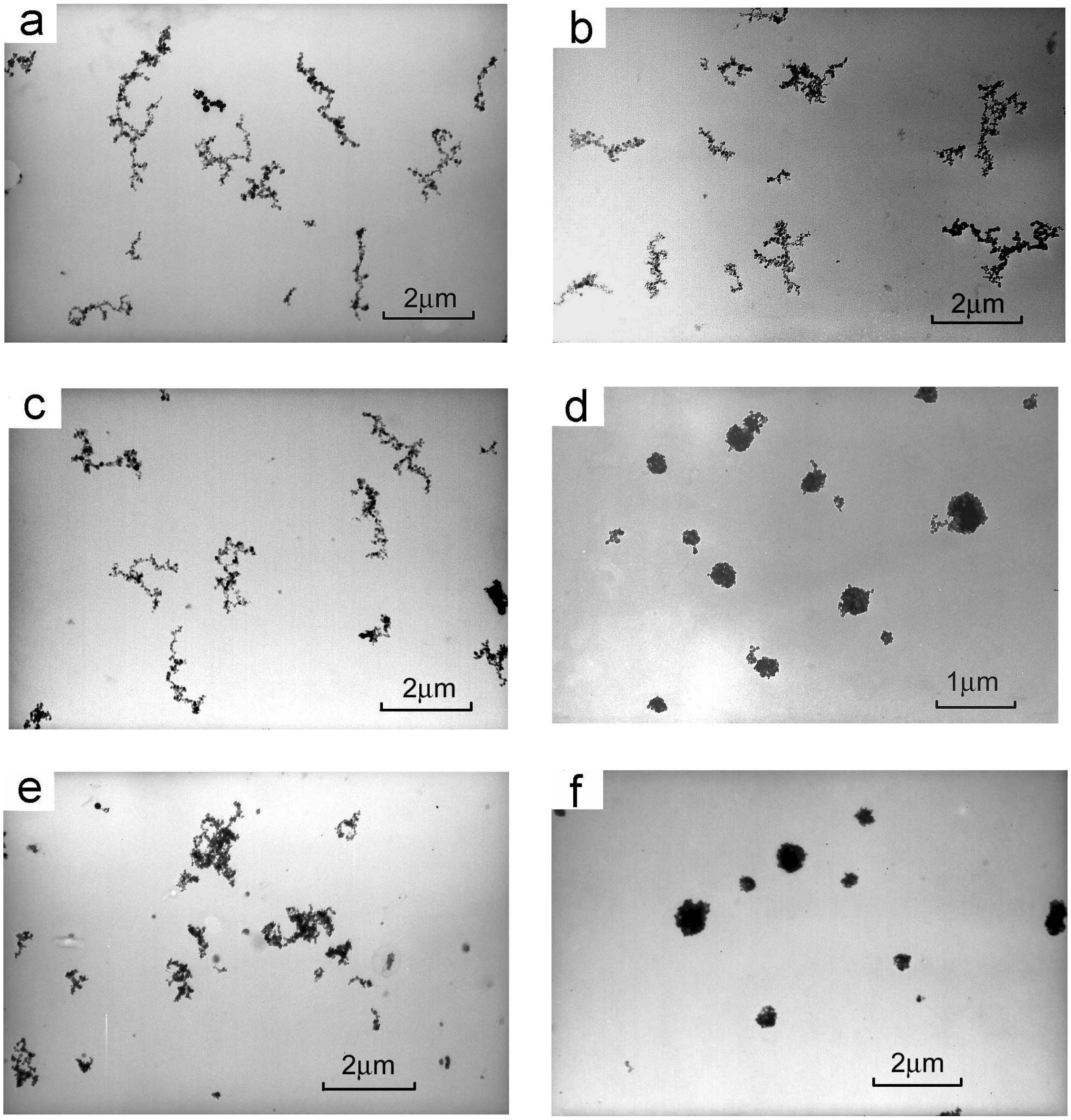

Figure 2. TEM images of soot particles: (a and b) hydrophobic soot (HBS), (c and d) hydrophilic soot (HLS), and (e and f) highly hydrophilic soot (HHLS). Figures 2a, 2c, and 2e are taken at RH = 10%, and Figures 2b, 2d, and 2f are taken at RH = 100%.

are denser than dry HBS (Figure 2a) and HLS (Figure 2c). This structural difference resulted from the relatively high content of glutaric acid, which provokes a microstructural rearrangement of the particles in the same way as water. It leads to the increase in fractal dimension of dry HHLS compared to dry HBS or HLS. Accordingly, the size spectrum of restructured particles moves toward the smaller sizes. After being exposed to wet conditions (RH = 100%), the HHLS (Figure 2f) and HLS (Figure 2d) become globular with similar fractal (Figures 3b and 3c) and size (Figures 4b and 4c) spectra.

[40] Note that the size of particles studied in this work exceeds the typical size of atmospheric soot because of analytical limitations. The mean mass diameter of long-lived natural BC particles (due to mixing with organic and inorganic substances, aging effects, and cloud processing) is within 0.1–0.3 μm (10–100 monomers per soot aggregate) [*Hendricks et al.*, 2004]. Nevertheless, in regions with heavy anthropogenic aerosol loading in the absence of wet deposition, disperse parameters of soot particles can essentially differ from spatiotemporal averaged size spectra. As an example, Figure 5 presents the mass distribution of well-aged soot sampled over the Indian Ocean during the dry season (February, 1997) in the Indian Ocean Experiment (INDOEX) [*Ramanathan et al.*, 2001b]. For comparison these data are complemented with mass distribution of HHLS particles (soot–glutaric acid mass ratio of 1) after undergoing wet restructuring (Figure 4c). As one can see, their disperse parameters are similar. As mentioned previously, the main goal of this work is to estimate how optical properties are affected by the mixing state of soot and humidity conditions. Within the framework of this objective, the absolute scales of size spectra are of only secondary importance.

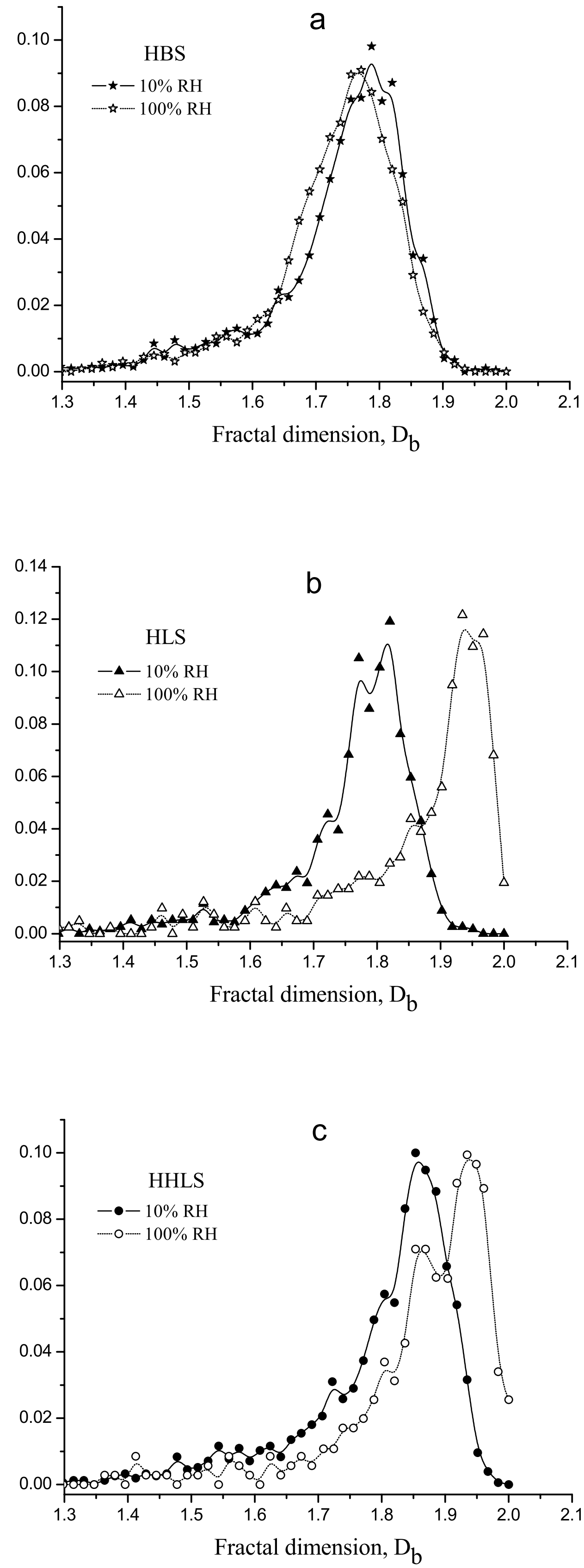

Figure 3. Fractal dimension distribution of soot particles: (a) hydrophobic soot (HBS), (b) hydrophilic soot (HLS), and (c) highly hydrophilic soot (HHLS). Solid symbols and solid curves, RH = 10%; open symbols and dashed curves, RH = 100%.

5.1.4. Microphysics Comparison of Different Soot Aggregates

[41] The averaged microphysical characteristics of particles are listed in Table 1 and confirm the microstructural rearrangement due to interaction with glutaric acid and water.

[42] For HBS, both 2-D and 3-D parameters are nearly the same. On the contrary, HLS with glutaric acid adsorbed at the surface is subject to strong restructuring. Specifically, the Ferret diameter d_F decreases approximately by a factor of 2 and the fractal dimension D_f increases by 20%. For the HHLS particles, the relative size decreases by 5% only because of volume condensation of glutaric acid and partial restructuring of micron size particles (Figure 4b). D_f grows by 20% in the same way as for the HLS particles.

[43] For the original fractal-like particles, both 2-D and 3-D structural parameters, D_f and k_f, are in a good agreement with results reported by *Koylu et al.* [1995]. After restructuring, however, their internal structure differs from the fractal one. Therefore the algorithms used to transform the 2-D images of fractal particles into 3-D structural properties of globular objects are not absolutely correct and were not employed for the reconstruction of structural parameters of the HLS and HHLS particles at RH = 100%. As seen from Table 1, there is a difference between fractal dimensions of D_f and D_b resulting from different averaging procedures. The net D_f value is the slope of relationship (10) plotted on a log-log scale, while the net D_b value is determined from averaging the fractal dimension distribution.

[44] Hydrophilic soot particles in the moist atmosphere act as condensation nuclei for water vapor, which leads to formation of an internally mixed aero-disperse system. Hence it is reasonable to expect that optical properties of such a system will differ substantially from the properties of "dry" soot.

5.2. Optical Coefficients of HBS and HLS Particles: Mass Concentration Dependence

[45] Figure 6 shows the volumetric optical coefficients as a function of mass concentration of hydrophobic and hydrophilic soot particles at RH = 10% and RH = 100%. In spite of high mass concentration values, the optical coefficients are linear functions and point to the adaptability of single scattering approach and to the Beer-Lambert law as a consequence. It is apparent that the optical parameters of the hydrophobic soot depend weakly on the humidity condition inside the cell over the whole mass concentration range. The hydrophilic soot extinction (Figure 6a) and scattering (Figure 6b) coefficients differ markedly from dry to saturated conditions. This difference correlates with structural rearrangement of HLS particles (see Figures 2d, 3b, and 4b) at RH = 100% due to deliquesence of hydrophilic particles. According to equation (16), growth factor of HLS particles ($m_{G.A.}/m_{soot}$, g_{sol} = 3.802) equals 1.25 at saturated humidity values. The hydration shell term (18)

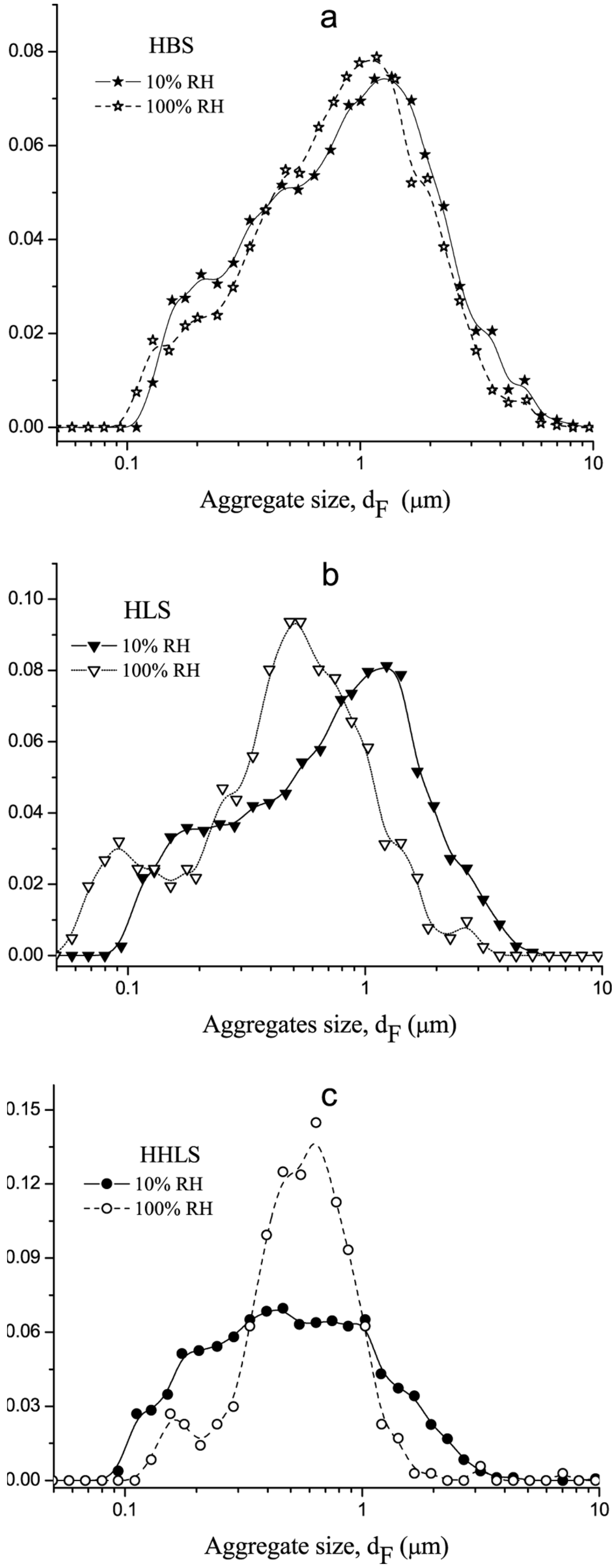

Figure 4. Normalized soot particle size distribution: (a) hydrophobic soot (HBS), (b) hydrophilic soot (HLS), and (c) highly hydrophilic soot (HHLS) with glutaric acid to soot mass ratio of 1:1. Solid curves, RH = 10%; dashed curves, RH = 100%.

corresponds to $H_{water\ shell}/R_{soot\ core} = 0.25$. Because of this water shell the scattering coefficient of HLS noticeably increases (Figure 6b). At the same time, the absorption coefficients of HBS and HLS particles are nearly constant (Figure 6c). Figure 6d shows calculated SSA values. The SSA of HLS particles increases almost twofold in saturated air. Table 2 summarizes the specific mass optical coefficients averaged over all of the soot mass concentrations. The extinction, scattering and adsorption coefficients were derived as slope ratios of the dependencies presented in Figure 6.

[46] For HBS dry particles, the average SSA value is equal to 0.30 ± 0.07, which is slightly higher than the 0.220 ± 0.007 value obtained by *Mulholland and Choi* [1998]. Apart from the experimental uncertainties, this deviation may be the result of partial watering of HBS particles even in the range of low humidity. Additional evidence in favor of this assumption is presented by the water adsorption isotherm obtained with the sorptograph technique. Figure 7 illustrates water adsorption properties of initial HBS particles used in the reported measurements. It is seen that the equilibrium mass of adsorbed water continuously increases with the increase in relative humidity. Assuming that water molecules cover the surface of a particle uniformly, the specific surface of soot is 31.5 m^2/g. Since the diameter of a water molecule is approximately 0.3 nm, the amounts of adsorbed water at RH = 10% and RH = 95% correspond to liquid-like films of about 1 and 5 monolayers, respectively. It is quite possible, therefore, that a relative SSA increase of 10% at RH = 100% versus RH = 10% (Table 2) is caused by water adsorption on the soot impurities that are a byproduct of the initial soot production by the acetylene burner.

5.3. Optical Coefficients of HBS and HLS Particles: Number Concentration Dependence

[47] Figure 8 reports the experimental results obtained for HBS and HLS particles for different number concentrations. Similar to the mass concentration measurements, the optical coefficients of hydrophilic soot at saturated conditions exhibit noticeable increases in extinction (Figure 8a) and scattering (Figure 8b) coefficients compared to the dry particles. At the same time, the absorption coefficients are nearly independent of humidity. For concentrations exceed-

Table 1. Microstructural Rearrangement Parameters for Hydrophobic, Hydrophilic, and Highly Hydrophilic Soot Particles as a Function of Relative Humidity[a]

	RH = 10%			RH = 100%		
Structural Parameters	HBS	HLS	HHLS	HBS	HLS	HHLS
		2-D				
Ferret diameter d_F, μm	1.18	0.95	0.68	1.06	0.58	0.64
Gyration radius R_g, μm	0.38	0.31	0.22	0.35	0.19	0.21
Mass fractal dimension D_f	1.46	1.47	1.60	1.44	1.75	1.92
Prefactor k_f	9.57	8.89	8.86	8.72	7.01	7.95
Box fractal dimension D_b	1.74	1.76	1.80	1.73	1.86	1.86
		3-D				
Gyration radius R_g, μm	0.48	0.38	0.27	0.43		
Fractal dimension D_f	1.59	1.60	1.75	1.57		
Prefactor k_f	9.58	8.83	8.51	8.70		

[a] HBS, hydrophobic soot particles; HLS, hydrophilic soot particles; HHLS, highly hydrophilic soot particles; RH, relative humidity. The 3-D parameters are reconstructed on the basis of 2-D TEM images.

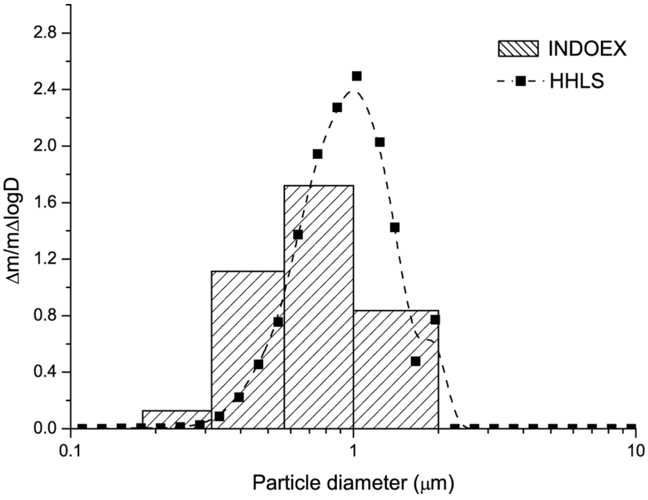

Figure 5. Normalized soot particle mass distribution. The histogram shows the impactor measurements obtained during INDOEX [*Ramanathan et al.*, 2001b]. Solid symbols and dashed curve represent the HHLS mixed particles with glutaric acid to soot mass ratio of 1:1 after wet restructuring.

ing 10^6/cm^3, extinction and scattering coefficients are a linear function of number concentration. For the smaller concentrations, the optical coefficients gradually move away from the linear line. Similar behavior of HLS particles was observed for the low mass concentrations (Figures 6a and 6b). Figure 8d presents the SSA values corresponding to the range of linear change of extinction and scattering coefficients. As one can see, the HLS particle SSA exceeds that of dry particles by a factor of 2. Furthermore, SSA for both hydrophobic and hydrophilic particles tends to increase with decreasing number concentration. This can be explained by an intense adsorption and condensation of water on soot particles due to the deficit of other condensation nuclei; that is, the increase of water shells around the particles compensates for the reduction of their concentration. The average optical cross sections and SSA are listed in Table 2. Reported SSA values are in good agreement with data derived from mass concentration measurements.

[48] Overall, comparison of optical properties (Figure 6, Figure 8, and Table 2) and microstructural rearrangements (Figure 2) of HBS and HLS particles clearly shows that observed differences occur because of water uptake on the hydrophilic particles. A hydration shell with a relative thickness of 25% provides an increase of scattering by more than a factor of 2, while the absorption is independent of the particle structure and the humidity conditions.

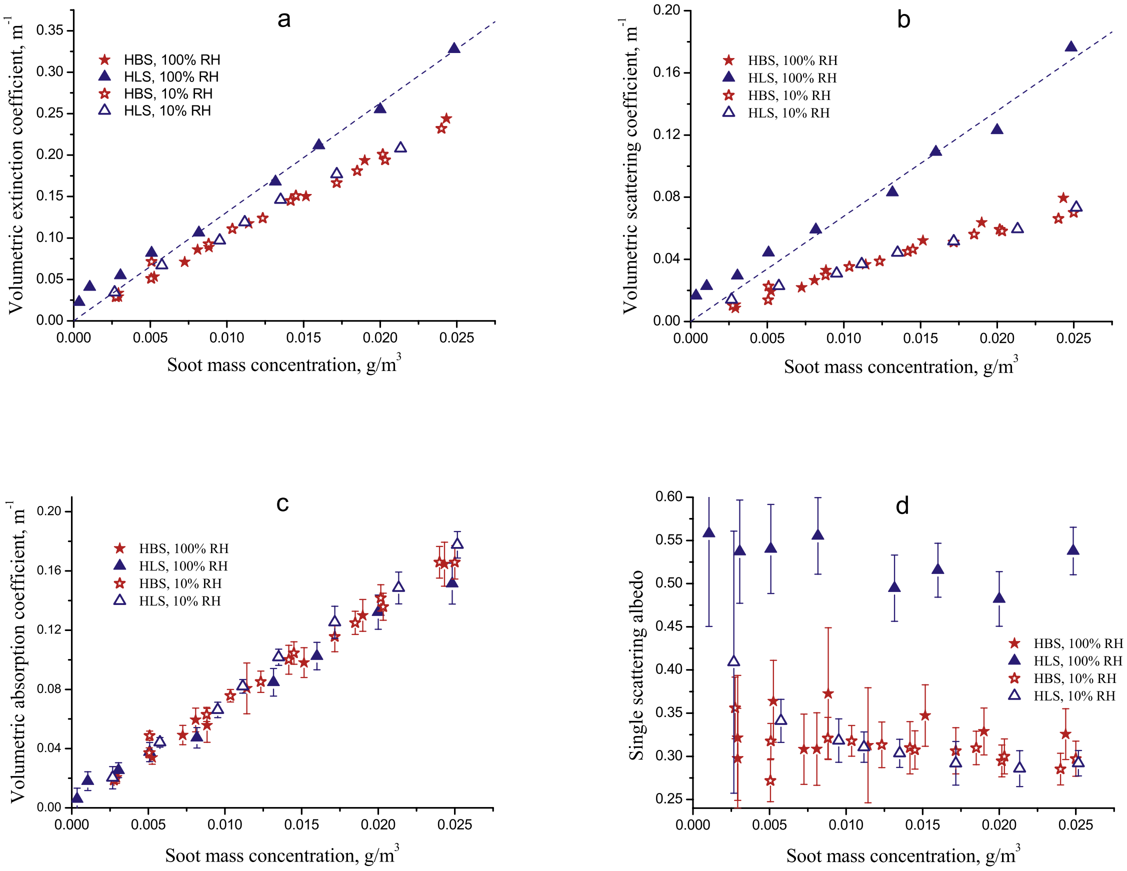

Figure 6. Volumetric (a) extinction, (b) scattering, and (c) absorption coefficients and (d) single-scattering albedo of hydrophobic (HBS, shown in red) and hydrophilic (HLS, shown in blue) soot versus volume mass concentration. Open symbols, RH = 10%; solid symbols, RH = 100%.

Table 2. Optical Coefficients of Soot Particles Derived From Measured Mass and Number Concentration[a]

		Mass Concentration Measurements				Number Concentration Measurements			
		Specific Coefficients, m^2/g				Cross Section, 10^{-10} cm^2			
RH, %	Type of Soot	Extinction	Scattering	Absorption	SSA	Extinction	Scattering	Absorption	SSA
100	HBS	10.1 ± 0.2	3.3 ± 0.2	6.8 ± 0.2	0.33 ± 0.07	7.7 ± 0.7	2.5 ± 0.3	5.1 ± 0.7	0.33 ± 0.06
100	HLS	13.2 ± 0.5	6.8 ± 0.4	6.4 ± 0.3	0.52 ± 0.07	9.1 ± 0.8	4.8 ± 0.5	4.3 ± 0.5	0.53 ± 0.10
10	HBS	9.8 ± 0.2	3.0 ± 0.2	6.9 ± 0.2	0.30 ± 0.07	6.9 ± 0.6	2.1 ± 0.2	4.9 ± 0.7	0.30 ± 0.06
10	HLS	10.2 ± 0.3	3.0 ± 0.2	7.2 ± 0.2	0.29 ± 0.07	7.1 ± 0.6	2.1 ± 0.2	4.9 ± 0.6	0.30 ± 0.06

[a] The value following the plus or minus sign is the standard deviation for ensemble measurements.

5.4. Single Aggregate

[49] Both optical measurements and TEM analysis allow an estimate of the average number of particles per aggregate. At first, the measured absorption cross sections were used. On the basis of the results by *Nelson* [1989] and *Chen et al.* [1990] we assume that absorption is not affected by aggregation

$$\mathrm{C^a_{abs}} = \mathrm{N_{opt}C^p_{abs}}, \tag{20}$$

where N_{opt} is the number of particles per aggregate, C^a_{abs}, C^p_{abs} are the absorption cross section of an aggregate and primary particle, respectively. Absorption cross section of primary particles was found using the Mie theory in the Raleigh limit [*Koylu and Faeth*, 1994].

[50] On the other hand, the number of particles per aggregate may be estimated on the basis of TEM analysis of 2-D projection images as

$$N_{TEM} = \frac{S^a_{mean}}{S^p_{mean}}. \tag{21}$$

Here, S^a_{mean} and $S^p_{mean} = \pi d_p^2/4$ are the average projection areas of an aggregate and primary particle, respectively. d_p is the primary particle diameter equal to 41 ± 8 nm. Table 3 presents the average values of number of particles per aggregate obtained keeping the fractal structure of soot constant for various humidity conditions. A good agreement between N_{opt} and N_{TEM} confirms the robustness of the approach used to measure the optical cross sections and structure parameters of the soot particles.

5.5. Optical Properties of HHLS Particles

[51] As discussed earlier, the surface modification of soot aerosol results in different optical coefficients. The degree of modification depends on the amount of glutaric acid adsorbed (adjusted by changing the temperature in the evaporator), soot particle concentration (number of condensation nuclei), and interaction time. By changing these parameters, glutaric acid to soot mass ratio can be set to any value in the 0.02 to 2 range. In practice, this ratio was adjusted by changing the soot volume flow through the mixer (Figure 1). The relatively high concentration of glutaric acid vapor results in the volume of condensation on the soot. After interaction with glutaric acid, the soot particles are internally mixed and the optical properties are a function of glutaric acid to soot mass ratio. Figure 9 shows the optical parameters of HHLS at RH = 10% as a function of the relative thickness of the glutaric acid shell (equation (14)) plotted on a log scale. Glutaric acid does not absorb radiation in visible spectrum; therefore an increase in shell thickness leads to an increase of the scattering cross section (Figure 9b), extinction cross section (Figure 9a), and SSA (Figure 9d). It is interesting that the absorption cross section tends to increase after being coated with a glutaric acid shell (Figure 9c). The maximum of absorption is 34%, although one can see this growth is within measurement errors. Note that a similar enhancement of the absorption coefficient of 35% has been observed by *Schnaiter et al.* [2003] for a spark discharged soot with a thin organic coating at λ = 473 nm.

[52] The change in optical properties is very apparent with the addition of hydrophilic material in the HHLS particles under saturated humidity conditions. Figure 10 shows an example of how optical depth and normalized scattering depend on the transformation of hydrophobic to highly hydrophilic soot. As one can see, extinction and scattering of HHLS particles grow dramatically in the water vapor saturated air. Simultaneously, the background noise increases as well because of the formation of water droplets on the hygroscopic particles.

[53] Figure 11 shows the optical parameters of HHLS at RH = 100% as a function of hydration shell thickness, which was calculated using equation (18). Presented data demonstrate a strong growth in scattering and extinction cross sections. Furthermore, it is clearly seen that the absorption cross section (Figure 11c) also increases.

[54] To demonstrate the influence of humidity conditions on the optical properties of the mixed particles, the cross sections results are presented using an enhancement factor

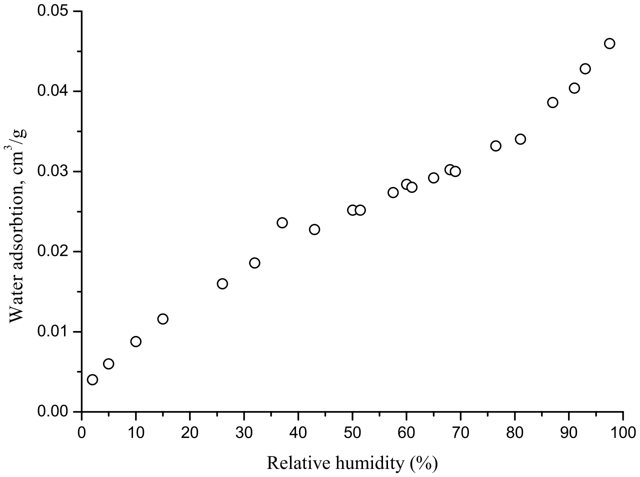

Figure 7. Volume of water absorbed at the surface of the acetylene soot as a function of relative humidity.

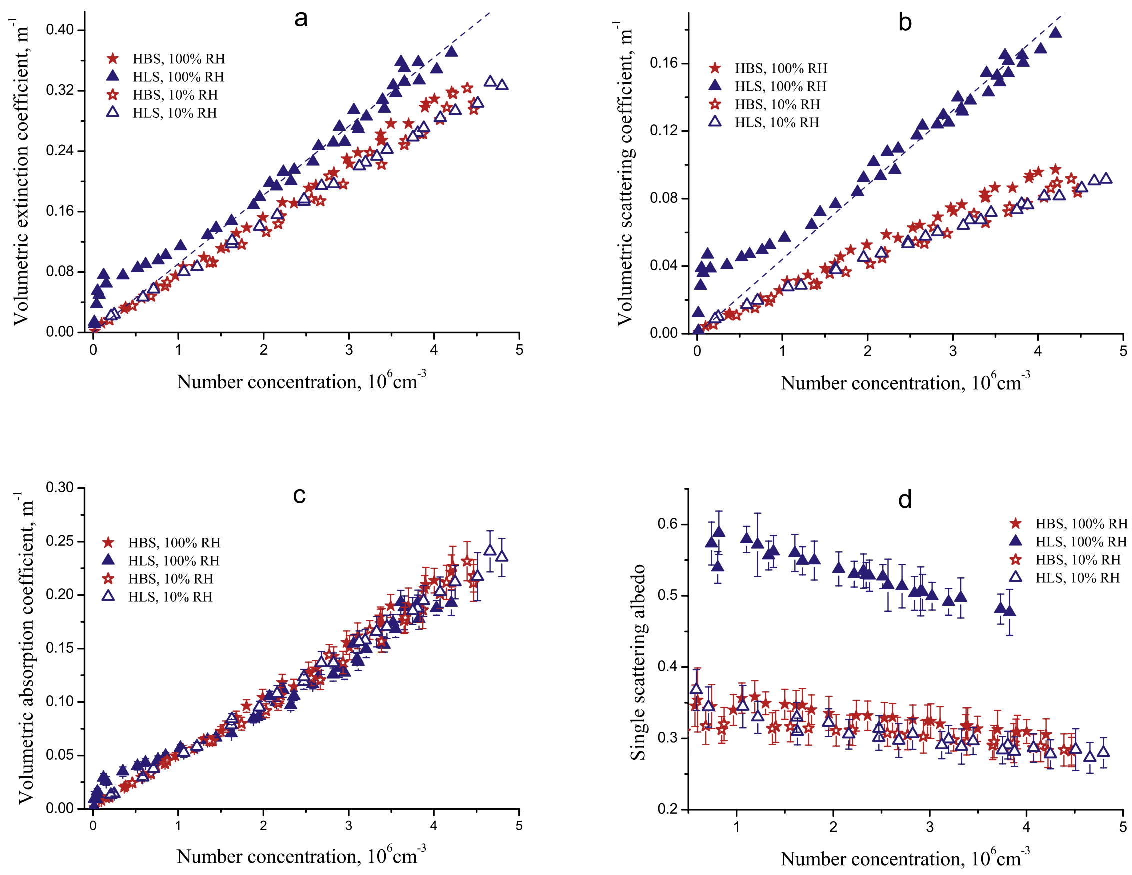

Figure 8. Volumetric (a) extinction, (b) scattering, and (c) absorption coefficients and (d) single-scattering albedo of hydrophobic (HBS, shown in red) and hydrophilic (HLS, shown in blue) soot particles versus number concentration. Open symbols, RH = 10%; solid symbols, RH = 100%.

$\chi = C_{i,\mathrm{HHLS}}(\mathrm{RH} = 100\%)/C_{i,\mathrm{HBS}}(\mathrm{RH} = 100\%)$ where *i* refers to *ext*, *scat* and *abs*. The results normalized in this way are shown in Figure 12. Consequently, the scattering enhancement factor becomes 34 ± 5. As a result, the SSA increases to 0.85 (Figure 11d), and the absorption enhancement factor for HHLS particles increases to 3.5 ± 1.0 (Figure 12); that is, a nonabsorbing shell around the soot core leads to an increase in absorption. This result is in good agreement with the values of 2.5–4.0 theoretically predicted by *Fuller et al.* [1999] for soot particles (radii ≥ 0.2 μm) positioned within nonabsorbing sulfate droplets.

6. Atmospheric and Climatic Implications

[55] The objective of this study was to use optical measurements and TEM analysis to investigate how complex interactions of soot particles with water vapor affect solar energy absorption. We found that hydrophobic soot exhibits no substantial difference in either optical properties or structural rearrangement under dry and humid conditions, while the optical properties of hydrophilic soot are strongly impacted by water vapor. According to the TEM analysis, the hydrophilic soot undergoes substantial restructuring in the humid atmosphere, which results in a very strong impact on the optical properties of soot. Under saturated conditions, soot particles with a surface modified by one monolayer of glutaric acid acquire an increase in hydration shell radius of ~25% and thus scatter light more strongly by a factor of 2.3 as compared to dry particles. At the same time, the absorption coefficients are insensitive to surface modification and humidity conditions. Further increase in the glutaric acid mass deposited on soot particles results in much more

Table 3. Average Number of Primary Particles per Fractal-like Soot Aggregate Obtained on the Basis of Optical Measurements at 635 nm and TEM Analysis

	HBS, 10% RH	HBS, 100% RH	HLS, 10% RH
d_p, nm	41	41	41
C^p_{abs}, cm^2	1.59×10^{-12}	159×10^{-12}	159×10^{-12}
C^a_{abs}, cm^2	4.85×10^{-10}	5.15×10^{-10}	5.10×10^{-10}
N_{opt}	175	185	183
S_{mean}, μm^2	0.29	0.28	0.26
N_{TEM}	221	211	195
$\lvert N_{TEM} - N_{opt}\rvert/N_{TEM}$	0.21	0.12	0.06

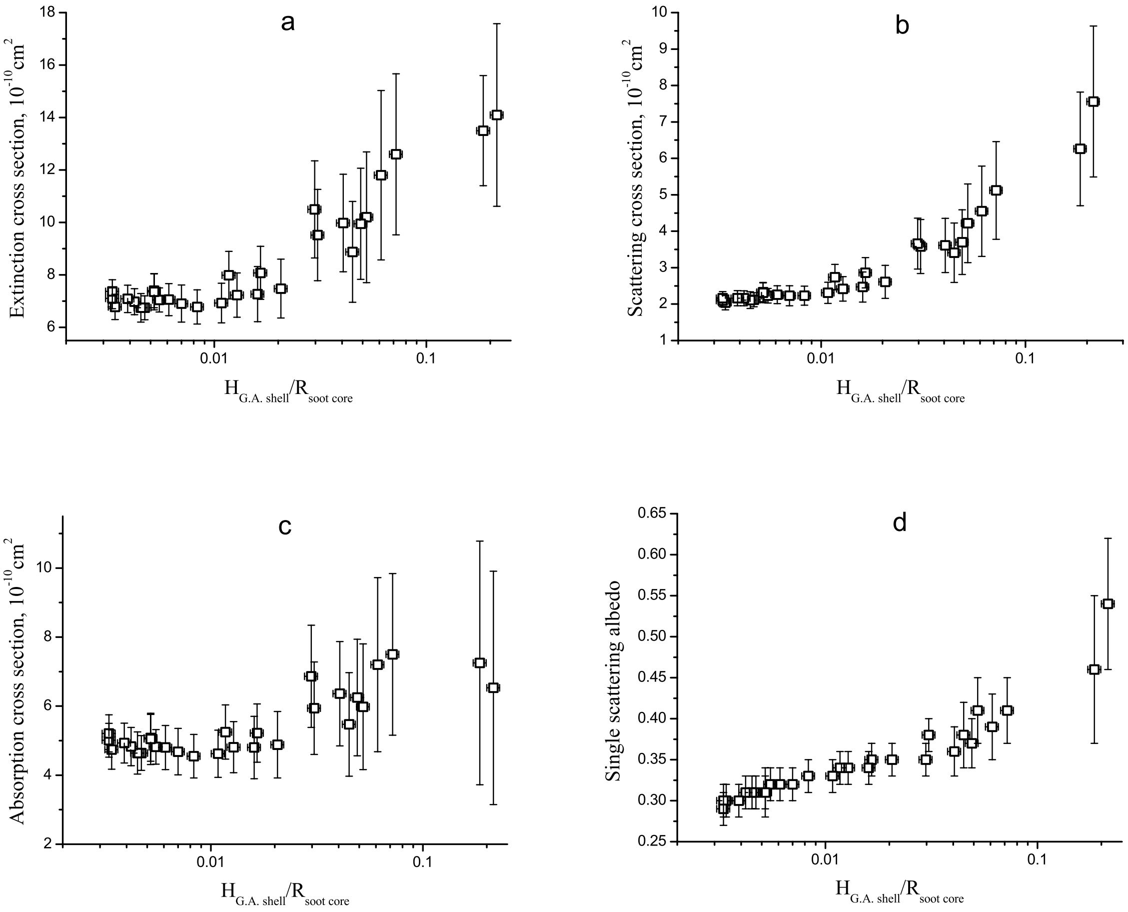

Figure 9. (a) Extinction, (b) scattering, and (c) absorption cross sections and (d) single-scattering albedo of highly hydrophilic soot (HHLS) particles versus relative thickness of glutaric acid shell around soot core at RH = 10%.

intensive condensation of the water vapor leading to the formation of droplets. The host droplets exhibit not only a strong increase in scattering, but also an appropriate increase in absorption. In particular, when the size of the host droplet exceeds the size of soot core by a factor of 4, the enhancement factor of scattering and of absorption with respect to hydrophobic particles amounts to 34 ± 5 and 3.5 ± 1.0, respectively. As discussed below, these results have significant implications for our understanding of the solar radiative forcing of the climate system due to clouds and aerosols.

[56] The observed increase in scattering and absorption caused by the condensation of saturated water vapor onto hygroscopic soot nuclei confirms the active role of organic compounds in the formation of haze and polluted clouds. These results are in a good agreement with laboratory experiments reported earlier by *Cruz and Pandis* [1997], *Corrigan and Novakov* [1999], *Prenni et al.* [2001, 2003], *Kumar et al.* [2003], and *Mikhailov et al.* [2004]. In this paper, however, we have made one important step further by linking chemical and microphysical laboratory experiments with a comprehensive set of optical observations and have demonstrated an increase in absorption by the soot–water drop agglomerates. Our study, therefore, has bridged the gap between the earlier laboratory experiments and theoretical predictions of the excess absorption by soot trapped

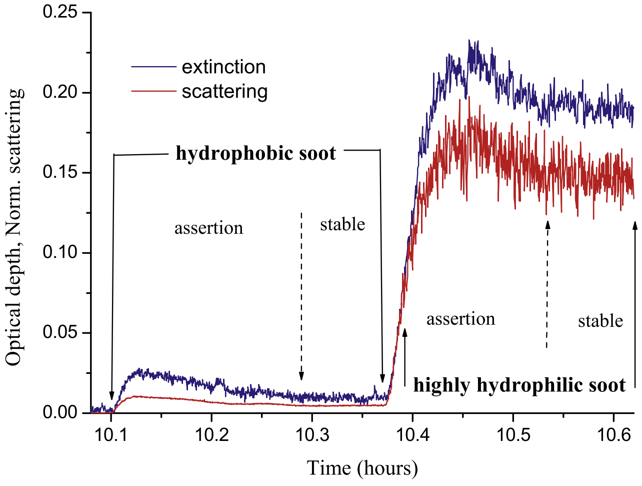

Figure 10. Temporal variations of optical depth and normalized scattering of hydrophobic and highly hydrophilic soot particles. Glutaric acid to soot mass ratio is 1:1, and RH = 100%.

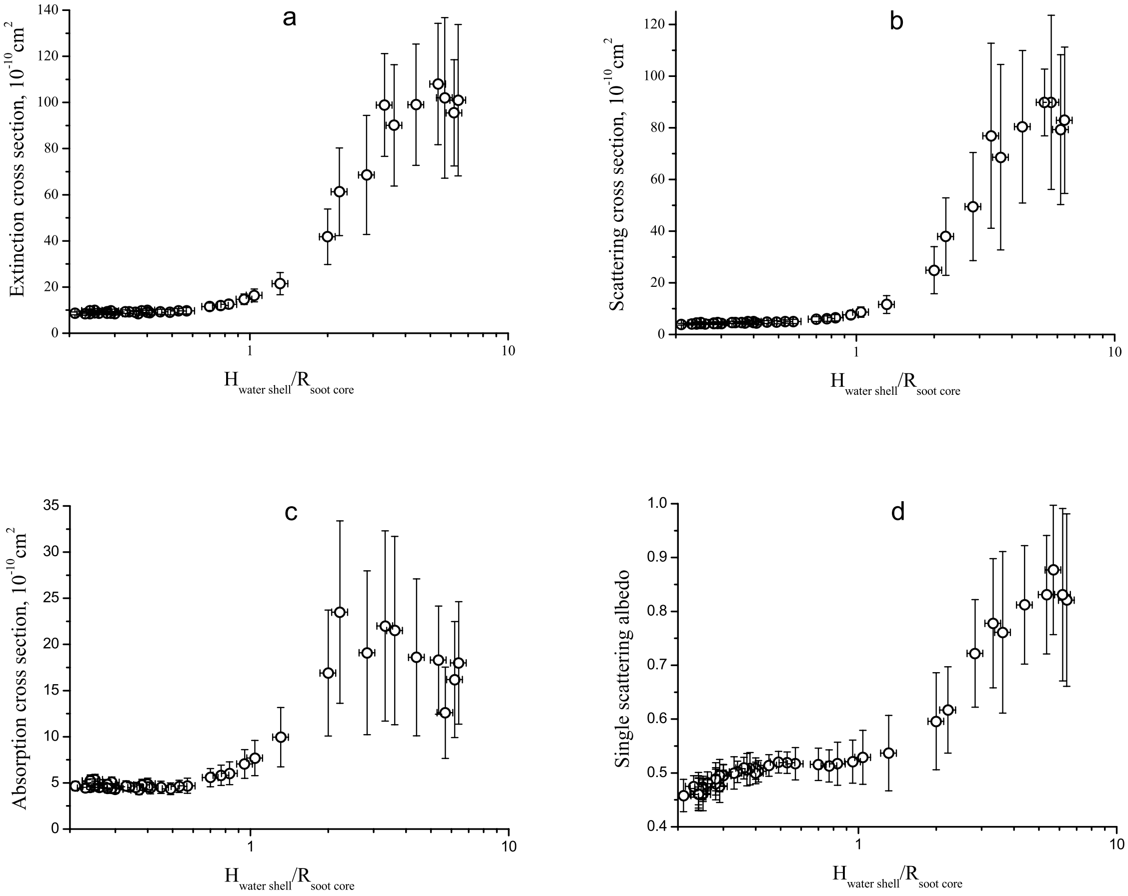

Figure 11. (a) Extinction, (b) scattering, and (c) absorption cross sections and (d) single-scattering albedo of highly hydrophilic soot (HHLS) particles versus relative thickness of water shell around the soot core at RH = 100%.

inside sulfate particles or water droplets [e.g., *Chylek and Hallett*, 1992; *Fuller et al.*, 1999; *Markel and Shalaev*, 1999]. Specifically, we have shown critical importance of OC in regulating the solar energy absorption by BC in cloud drops.

[57] The laboratory evidence for the enhancement of solar absorption within cloud drops nucleated by soot raises new interest in the so-called excess (or anomalous) absorption phenomenon [e.g., *Ramanathan and Vogelmann*, 1997]. Observed values of solar absorption since the 1950s have almost always exceeded theoretical and model values. The magnitude of this excess absorption (i.e., observed minus theoretical absorption) on climatologically relevant time-scales and spatial scales was quantified recently (1990s) by six independent studies, to be about 25 W m^{-2} (i.e., 8% of incident solar radiation) (see summary given by *Ramanathan and Vogelmann* [1997]). Recent field experiments [*Ramanathan et al.*, 2001b; *Conant et al.*, 2003] suggest that absorption by aerosols consisting of organics and elemental black carbon can explain as much as 4 to 5 Wm^{-2} of the excess absorption (see global summary given by *Ramanathan et al.* [2001a]), while another 2 to 5 Wm^{-2} is likely due to modeling deficiencies in water vapor absorption resulting from poor treatment of continuum absorption and incorrect line parameters [*Ramanathan and Vogelmann*, 1997; *Sierk et al.*, 2004]. The question of cloudy sky absorption has not been resolved satisfactorily. This study raises the possibility that cloudy skies containing sooty aerosols can significantly enhance atmospheric solar absorption. Further laboratory studies with more representative atmospheric organic species (such as oxalic acid) need to be conducted before this important issue can be addressed.

[58] As mentioned earlier, the understanding of the role of soot in regulating cloud albedo (i.e., all-sky direct forcing, semi-direct forcing and indirect forcing combined) constitutes a fundamental challenge to the modern theory of climate [e.g., *Ramanathan et al.*, 2001a; *Anderson et al.*, 2003]. The intense solar heating by soot and soot-containing aerosols can lead to evaporation of cumulus and stratus clouds resulting in more solar radiation reaching the surface, which can, in turn, offset the direct and the indirect aerosol forcing [*Nenes et al.*, 2002]. The cloud evaporation effect of soot depends critically on SSA of cloud drops in polluted clouds. The uncertainty in understanding climate change also arises from the effects of aerosols on cloud formation and subsequent indirect radiative forcing. In order to quantify the contribution of soot to all three types of forcing, we need to integrate aerosol data, laboratory experiments and aerosol radiative forcing estimates.

[59] BC and OC filter samples are routinely collected during aerosol field campaigns to be analyzed using various

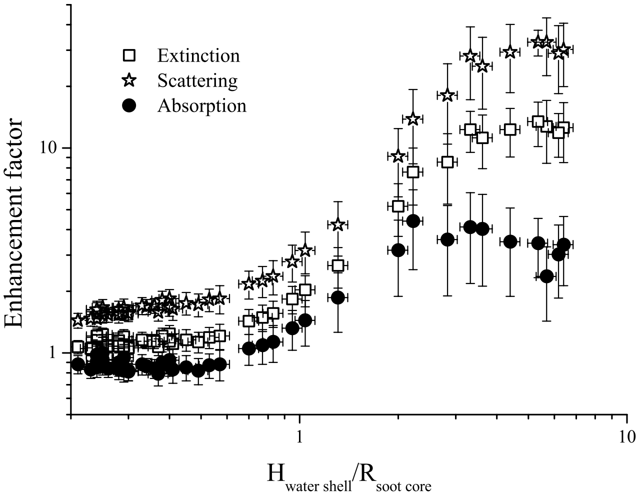

Figure 12. Enhancement factor of highly hydrophilic soot at RH = 100% versus relative thickness of water shell.

techniques [e.g., *Schauer et al.*, 2003], whereas recent emission data [*Bond et al.*, 2004] provide global coverage of BC and primary OC particles emitted from combustion. The BC/OC data along with gaseous (i.e., carbon monoxide) and aerosol chemical data can therefore be used to identify the sources and to quantify hygroscopic properties of soot and soot-containing aerosol and chemical composition organic and inorganic compounds associated with soot. The state of the mixture of aged aerosol derived from chemical analysis and TEM imagery will provide another set of constraints, so that model particles generated in the laboratory match those of the ambient atmospheric aerosol. The laboratory experiments designed in such a way will result in parameterization of aerosol microphysical processes and will substantially improve the climate models predictive capabilities with respect to aerosol forcing under cloudy skies.

[60] **Acknowledgment.** This work was supported by the Russian Fund for Basic Research grant 05-05-64756 and University of California Pacific Rim Research grant 2-T-PRRP-6-145.

References

Ackerman, A. S., O. B. Toon, D. E. Stevens, A. J. Heymsfield, V. Ramanathan, and E. J. Welton (2000), Reduction of tropical cloudiness by soot, *Science*, *288*, 1042–1047.

Anderson, T. L., R. J. Charlson, S. E. Schwartz, R. Knutti, O. Boucher, H. Rodhe, and J. Heintzenberg (2003), Climate forcing by aerosols: A hazy picture, *Science*, *300*, 1103–1104.

Baron, P. A., and K. Willeke (Eds.) (2001), *Aerosol Measurement: Principles, Techniques, and Applications*, 2nd ed., 1131 pp., Wiley-Interscience, New York.

Bohren, C. F., and D. R. Huffman (1998), *Absorption and Scattering of Light by Small Particles*, 544 pp., John Wiley, Hoboken, N. J.

Bond, T. C., D. G. Streets, K. F. Yarber, S. M. Nelson, J.-H. Woo, and Z. Klimont (2004), A technology-based global inventory of black and organic carbon emissions from combustion, *J. Geophys. Res.*, *109*, D14203, doi:10.1029/2003JD003697.

Cai, J., N. Lu, and C. M. Sorensen (1993), Comparison of size and morphology of soot aggregates as determined by light scattering and electron microscope analysis, *Langmuir*, *9*, 2861–2867.

Chen, H. Y., M. F. Iskander, and J. E. Penner (1990), Light sacattering and absorption by fractal agglomerates and coagulations of smoke aerosols, *J. Mod. Opt.*, *2*, 171–181.

Chylek, P., and J. Hallett (1992), Enhanced absorption of solar radiation by cloud droplets containing soot particles in their surface, *Q. J. R. Meteorol. Soc.*, *118*, 167–172.

Chylek, P., G. B. Lesins, G. Videen, J. G. D. Wong, R. G. Pinnick, D. Ngo, and J. D. Klett (1996), Black carbon and absorption of solar radiation by clouds, *J. Geophys. Res.*, *101*, 23,365–23,371.

Conant, W. C., J. H. Seinfeld, J. Wang, G. R. Carmichael, Y. H. Tang, I. Uno, P. J. Flatau, K. M. Markowicz, and P. K. Quinn (2003), A model for the radiative forcing during ACE-Asia derived from CIRPAS Twin Otter and R/V *Ronald H. Brown* data and comparison with observations, *J. Geophys. Res.*, *108*(D23), 8661, doi:10.1029/2002JD003260.

Corrigan, C. E., and T. Novakov (1999), Cloud condensation nucleus activity of organic compounds: A laboratory studies, *Atmos. Environ.*, *33*, 2661–2668.

Cruz, C. N., and S. N. Pandis (1997), A study of the ability of pure secondary organic aerosol to act as cloud condensation nuclei, *Atmos. Environ.*, *31*, 2205–2214.

Dobbings, R. A., G. W. Mulholland, and N. P. Bryner (1994), Comparison of a fractal smoke optics model with light extinction measurements, *Atmos. Environ.*, *28*, 889–897.

Feder, J. (1988), *Fractals*, Springer, New York.

Finlayson-Pitts, B. J., and J. N. Pitts Jr. (2000), *Chemistry of Upper and Lower Atmosphere*, Elsevier, New York.

Fuller, K. A., W. C. Malm, and S. M. Kreidenweis (1999), Effects of mixing on extinction by carbonaceous particles, *J. Geophys. Res.*, *104*, 15,941–15,954.

Fuzzi, S., et al. (2001), A samplified model of the water soluble organic component of atmospheric aerosols, *Geophys. Res. Lett.*, *28*, 4079–4082.

Greg, K., and X. Sing (1984), *Adsorption, Specific Surface and Porosity* (in Russian), 178 pp., Nauka, Moscow.

Guazzotti, S. A., et al. (2003), Characterization of carbonaceous aerosols outflow from India and Arabia: Biomass/biofuel burning and fossil fuel combustion, *J. Geophys. Res.*, *108*(D15), 4485, doi:10.1029/2002JD003277.

Hansen, J., M. Sato, and R. Ruedy (1997), Radiative forcing and climate response, *J. Geophys. Res.*, *102*, 6831–6864.

Haywood, J. M., D. L. Roberts, A. Slingo, J. M. Edwards, and K. P. Shine (1997), General circulation model calculations of the direct radiative forcing by anthropogenic sulfate and fossil-fuel soot aerosol, *J. Clim.*, *10*, 1562–1577.

Hendricks, J., B. Karcher, A. Dopelheur, J. Feichter, U. Lohmann, and D. Baumgardner (2004), Simulating the global atmospheric black carbon cycle: A revisit to the contribution of aircraft emissions, *Atmos. Chem. Phys.*, *4*, 2521–2541.

Huebert, B. J., T. Bates, P. B. Russell, G. Shi, Y. J. Kim, K. Kawamura, G. Carmichael, and T. Nakajima (2003), An overview of ACE-Asia: Strategies for quantifying the relationships between Asian aerosols and their climatic impacts, *J. Geophys. Res.*, *108*(D23), 8633, doi:10.1029/2003JD003550.

Intergovernmental Panel on Climate Change (2001), *Climate Change 2001: Scientific Basis, Technical Summary of the Working Group I Report*, Cambridge Univ. Press, New York.

Jacobson, M. Z. (2000), A physically-based treatment of elemental carbon optics: Implications for global direct forcing of aerosols, *Geophys. Res. Lett.*, *27*, 217–220.

Jacobson, M. Z. (2001), Global direct radiative forcing due to multicomponent anthropogenic and natural aerosols, *J. Geophys. Res.*, *106*, 1551–1568.

Jayaraman, A., D. Lubin, S. Ramachandran, V. Ramanathan, E. Woodbridge, W. D. Collins, and K. S. Zalpuri (1998), Direct observations of aerosol radiative forcing over the tropical Indian Ocean during the January-February 1996 pre-INDOEX cruise, *J. Geophys. Res.*, *103*, 13,827–13,836.

Kinne, S., et al. (2003), Monthly averages of aerosol properties: A global comparison among models, satellite data, and AERONET ground data, *J. Geophys. Res.*, *108*(D20), 4634, doi:10.1029/2001JD001253.

Koylu, U. O., and G. M. Faeth (1994), Optical properties of overfire soot in buoyant turbulent diffusion flames at long residence times, *J. Heat Transfer*, *116*, 152–159.

Koylu, U. O., G. M. Faeth, T. L. Farias, and M. G. Carvalho (1995), Fractal and projected structure properties of soot aggregates, *Combust. Flame*, *100*, 621–633.

Kumar, P. P., K. Broekhuizen, and J. P. D. Abbatt (2003), Organic acids as cloud condensation nuclei: Laboratory studies of highly soluble and insoluble species, *Atmos. Chem. Phys.*, *3*, 949–982.

Lawrence, J., and P. Koutrakis (1996), Measurement and speciation of gas and particle phase organic acidity in an urban environment: 2. Analytical, *J. Geophys. Res.*, *101*, 9171–9184.

Lim, H. F., B. J. Turpin, L. M. Russell, and T. S. Bates (2003), Organic and elemental carbon measurement during ACE-Asia suggest a longer atmospheric lifetime for elemental carbon, *Environ. Sci. Technol.*, *37*, 3055–3061.

Liousse, C., H. Cachier, and S. G. Jennings (1993), Optical and thermal measurements of black carbon aerosol content in different environments: Variation of the specific attenuation cross section, *Atmos. Environ., Part A*, *27*, 1203–1211.

Mandelbrot, B. B. (1983), *The Fractal Geometry of Nature*, 468 pp., W. H. Freeman, New York.

Maria, S. F., L. M. Russell, B. J. Turpin, and R. J. Porcja (2002), FTIR measurement of functional groups and organic mass in aerosol samples over Caribbean, *Atmos. Environ.*, *36*, 5185–5196.

Maria, S. F., L. M. Russell, B. J. Turpin, R. J. Porcja, T. L. Campos, R. J. Weber, and B. J. Huebert (2003), Source signatures of carbon monoxide and organic functional groups in Asian Pacific Regional Aerosol Characterization Experiment (ACE-Asia) submicron aerosol types, *J. Geophys. Res.*, *108*(D23), 8637, doi:10.1029/2003JD003703.

Markel, V. M. (2002), The effects of averaging on the enhancement factor for absorption of light by carbon particles in microdroplets of water, *J. Quant. Spectrosc. Radiat. Transfer*, *72*, 765–774.

Markel, V. M., and V. M. Shalaev (1999), Absorption of light by soot particles in micro-droplets of water, *J. Quant. Spectrosc. Radiat. Transfer*, *63*, 321–339.

McDow, S. R., M. Jang, Y. Hong, and R. M. Kamens (1996), An approach to studying the effect of organic compounds on atmospheric aerosol photochemistry, *J. Geophys. Res.*, *101*, 19,593–19,600.

Mikhailov, E. F., S. S. Vlasenko, and A. A. Kiselev (2001), Optics and structure of carbonaceous soot aggregates, in *Optics of Nanostructured Materials*, edited by V. A. Markel and T. F. George, pp. 413–466, John Wiley, Hoboken, N. J.

Mikhailov, E. F., S. S. Vlasenko, I. A. Podgorny, V. Ramanathan, J. F. Safronova, and M. V. Oleinichenko (2003), Optical properties of soot–water droplet agglomerates: An experimental study, paper presented at 2003 European Aerosol Conference, Eur. Aerosol Assem., Madrid, Spain, 31 Aug. to 5 Sept.

Mikhailov, E. F., S. S. Vlasenko, R. Niessner, and U. Poschl (2004), Interaction of aerosol particles composed of protein and salts with water vapor: Hygroscopic growth and microstructural rearrangement, *Atmos. Chem. Phys.*, *4*, 323–350.

Mulholland, G. W., and N. P. Bryner (1994), Radiometric model of the transmission cell-resiprocal nephelometer, *Atmos. Environ.*, *28*, 873–887.

Mulholland, G. W., and M. Y. Choi (1998), Measurement of the mass specific extinction coefficient for acetylene and ethene smoke using the Large Agglomerate Optics Facility, paper presented at 27th International Symposium on Combustion, Combust. Inst., Boulder, Colo., 2–7 Aug.

Nelson, J. (1989), Test of a mean field theory for the optics of fractal clusters, *J. Mod. Opt.*, *36*, 1031–1057.

Nenes, A., W. C. Conant, and J. H. Seinfeld (2002), Black carbon radiative heating effects on cloud microphysics and implications for the aerosol indirect effect: 2. Cloud microphysics, *J. Geophys. Res.*, *107*(D21), 4605, doi:10.1029/2002JD002101.

Niessner, R., and C. Helsper (1985), Application of a multistep condensation nuclei counter as a detector for particle surface composition, *J. Aerosol Sci.*, *16*, 201–210.

Patterson, E. M., R. M. Duckworth, C. M. Wyman, E. A. Powell, and J. W. Gooch (1991), Measurement of the optical properties of the smoke emission from plastics, hydrocarbons, and other urban fuels for nuclear winter studies, *Atmos. Environ., Part A*, *25*, 2539–2552.

Peng, C. G., M. N. Chan, and C. K. Chan (2001), The hygroscopic properties of dicarboxylic and multifunctional acids: Measurements and UNIFAC predictions, *Environ. Sci. Technol.*, *35*, 4495–4501.

Pitchford, M. L., and P. H. McMurry (1994), Relationship between measured water vapor growth and chemistry of atmospheric aerosol for Grand Canyon, Arizona, in winter 1990, *Atmos. Environ.*, *28*, 827–839.

Prenni, A. J., P. J. DeMott, S. M. Kreidenweis, D. E. Sherman, L. M. Russell, and Y. Ming (2001), The effects of low molecular weight dicarboxylic acids on cloud formation, *J. Phys. Chem. A*, *105*, 11,240–11,248.

Prenni, A. J., P. D. DeMott, and S. M. Kriedenweis (2003), Water uptake of internally mixed particles containing ammonium sulphate and dicarbocylic acids, *Atmos. Environ.*, *37*, 4243–4245.

Ramanathan, V., and A. M. Vogelmann (1997), Greenhouse effect, atmospheric solar absorption and the Earth's radiation budget: From the Arrhenius/Langley era to the 1990s, *Ambio*, *26*(1), 38–46.

Ramanathan, V., P. J. Crutzen, J. T. Kiehl, and D. Rosenfeld (2001a), Aerosols, climate, and the hydrological cycle, *Science*, *294*, 2119–2124.

Ramanathan, V., et al. (2001b), The Indian Ocean Experiment: An integrated analysis of the climate forcing and effects of the Great Indo-Asian Haze, *J. Geophys. Res.*, *106*, 28,371–28,398.

Russell, L. M., S. F. Maria, and S. C. B. Myneni (2002), Mapping organic coatings on atmospheric particles, *Geophys. Res. Lett.*, *29*(16), 1779, doi:10.1029/2002GL014874.

Russell, P. B., P. V. Hobbs, and L. L. Stowe (1999), Aerosol properties and radiative effects in the United States east coast haze plume: An overview of the Tropospheric Aerosol Radiative Forcing Observational Experiment (TARFOX), *J. Geophys. Res.*, *104*, 2213–2222.

Samson, R. J., G. M. Mulholland, and J. W. Gentry (1987), Structural analysis of soot agglomerates, *Langmuir*, *3*, 272–281.

Satheesh, S. K., and V. Ramanathan (2000), Large differences in tropical aerosol forcing at the top of the atmosphere and Earth's surface, *Nature*, *405*, 60–63.

Saxena, P., and L. M. Hildemann (1996), Water-soluble organics in atmospheric particles: A critical review of the literature and application of thermodynamics to identify candidate compounds, *J. Atmos. Chem.*, *24*, 57–109.

Schauer, J. J., et al. (2003), ACE-Asia intercomparison of a thermal optical method for the determination of particle-phase organic and elemental carbon, *Environ. Sci. Technol.*, *37*, 993–1001.

Schnaiter, M., H. Horvath, O. Mohler, K.-H. Naumann, H. Saathoff, and O. W. Schock (2003), UV-VIS-NIR spectral optical properties of soot and soot-containing aerosols, *J. Aerosol Sci.*, *34*, 1421–1444.

Seinfeld, J. H., and S. N. Pandis (1998), *Atmospheric Chemistry and Physics: From Air Pollution to Climate Change*, John Wiley, Hoboken, N. J.

Sierk, B., S. Solomon, J. S. Daniel, R. W. Portmann, S. I. Gutman, A. O. Langford, C. S. Eubank, E. G. Dutton, and K. H. Holub (2004), Field measurements of water vapor continuum absorption in the visible and near-infrared, *J. Geophys. Res.*, *109*, D08307, doi:10.1029/2003JD003586.

Sorensen, C. M. (2001), Light scattering by fractal aggregates: A review, *Aerosol Sci. Technol.*, *35*, 648–687.

Sutugin, A. G., and N. A. Fuchs (1965), Coagulation rate of highly dispersed aerosols, *J. Colloid Sci.*, *20*, 492–500.

Tao, Y., and P. H. McMurry (1989), Vapor pressure and surface free energies of C14–C18 monocarboxylic acids and C5 and C6 dicarboxylic acids, *Environ. Sci. Technol.*, *23*, 1519–1523.

Twomey, S. (1977), The influence of pollution on the short-wave albedo of clouds, *J. Atmos. Sci.*, *34*, 1149–1152.

Wang, C. (2004), A modeling study on the climate impacts of black carbon aerosols, *J. Geophys. Res.*, *109*, D03106, doi:10.1029/2003JD004084.

Weingartner, E., H. Burtscher, and U. Baltensperger (1997), Hygroscopic properties of carbon and diesel soot particles, *Atmos. Environ.*, *31*, 2311–2327.

Yao, X., M. Fang, and K. Chan (2002), Size distributions and formation of dicarboxylic acids in atmospheric particles, *Atmos. Environ.*, *36*, 2099–2107.

C. E. Corrigan, I. A. Podgorny, and V. Ramanathan, Center for Atmospheric Sciences, Scripps Institution of Oceanography, University of California, San Diego, La Jolla, CA 92093, USA. (igor@fiji.ucsd.edu)

E. F. Mikhailov and S. S. Vlasenko, Atmospheric Physics Department, Research Institute of Physics, St. Petersburg State University, Petrodvorets, St. Petersburg, 198504 Russia.